Electron Transfer through Organic Molecules

ARTICLE *in* THE JOURNAL OF PHYSICAL CHEMISTRY B · SEPTEMBER 1999

Impact Factor: 3.3 · DOI: 10.1021/jp9921699

5 AUTHORS, INCLUDING:

Timothy D. Dunbar
3M
25 PUBLICATIONS **2,855** CITATIONS
SEE PROFILE

David L Allara
Pennsylvania State University
261 PUBLICATIONS **23,156** CITATIONS
SEE PROFILE

Paul S Weiss
University of California, Los Angeles
395 PUBLICATIONS **11,930** CITATIONS
SEE PROFILE

Electron Transfer through Organic Molecules

L. A. Bumm,[†] J. J. Arnold,[†] T. D. Dunbar,[‡] D. L. Allara,*[,§] and P. S. Weiss*[,†]

Departments of Chemistry and Materials Science and Engineering, The Pennsylvania State University, University Park, Pennsylvania 16802-6300

Received: June 28, 1999

Electron transfer through molecular frameworks is central to a wide range of chemical, physical, and biological processes. We demonstrate a means to measure electronically and to quantify electron transfer through organic molecules and films. We show quantitative agreement with universal values of electron transfer inferred from biological, electrochemical, photochemical, and related systems. Scanning tunneling microscopy was used to image adjacent chains and molecular terraces of different length alkanethiolates in an ordered self-assembled monolayer lattice on Au{111}. In electron transfer measurements using a scanning tunneling microscope, both the driving force and the electrode separation can be continuously varied. This allows independent electronic measurement of the molecular bridges through which electron transfer takes place. The differences between the measured topography in scanning tunneling microscopy and the physical heights of these molecules can be understood in terms of the transconductance through individual chains using a two-layer tunnel junction model.

Introduction

Many quantitative measurements of electron transfer efficiencies through molecular frameworks have been made.[1−35] These have generally applied optical spectroscopy,[4−9] electrochemistry,[10−15] or direct electronic measurements[16−26] to large ensembles of molecules. The values obtained are thus ensemble averages. Measurements of electron transfer through individual molecules are more difficult. Small ensembles of molecules have been measured using break junctions,[17] nanolithographically defined pores,[18] nanometer-scale contacts,[19] and nanometer-scale networks.[20] Carbon nanotubes are particularly amenable to single-molecule measurements because of their extreme lengths (micrometers). Measurements have been made of the molecular electronic properties on single-wall,[21] multiwall,[22−25] and ropes of single-wall[26] carbon nanotubes.

Understanding electron transfer at the molecular level will aid in developing molecular assemblies with unique properties and novel applications, such as photosynthetic systems[5,36] and molecular electronic devices.[37−43] In addition, measurements of the transconductances of contacts and of molecules will give us critical insight into the electronic couplings within and between molecules and at interfaces. Key to understanding electron transfer is the ability to make quantitative measurements on single molecules, features, or components. This will provide the capability to compare directly to inferred electron dynamics in biochemistry,[2,4,6,7,44] electrochemistry,[10−13] photochemistry,[5,36] and nanometer- and molecular-scale electronics.[37−43] In addition, we address how the scanning tunneling microscope is capable of imaging such "insulating" molecular structures and discuss the contrast mechanism in scanning tunneling microscopy (STM).

Scanning tunneling microscopy is ideally suited to make localized measurements of electron transfer through organic thin films because it interacts with the sample via electron tunneling and because of its high spatial resolution. We and others have used STM to measure electron transfer through individual molecules[27−30] and through atomic assemblies.[31,32] Atomic force microscopy also can be used when combined with a conducting tip.[25,33]

Scanned probe techniques have the advantage that the measurements are intrinsically localized to nanometer-scale areas. With them we can both spatially select and make direct electronic measurements of the molecules supported on a substrate. If the molecules are sufficiently separated, the scanning tunneling microscope can be used to select a single molecule for study. In STM, electrons tunnel through the gap between the tip and the sample. The tip−sample separation is typically adjusted to maintain a constant tunneling current while the tip is scanned across the surface. Such a constant current STM topograph convolves the electronic and physical structures of both the tip and the sample.[45,46] Unambiguously separating these contributions to the STM topography can only be achieved with the knowledge of one of these components. We do this by studying a well-defined organic thin film structure with molecularly sharp boundaries between regions of different film composition, as described in ref 47.

We are able to measure alkyl chain transconductance for a range of chain lengths and the contribution of the chemical contacts to this conductance. These experiments are performed as pairwise (or higher) combinations of molecular systems so as to eliminate the contributions and perturbations of the measurement systems which here is STM. In earlier work, we demonstrated the ability to measure single isolated molecules in a well-defined matrix.[27] This circumvents the difficulty encountered in electrodes defined by nanometer-scale contacts[17−19] and networks[20] in that no inference need be made as to the contents of the measurement junction. Rather, the contents are identified and selected directly by STM.[27,28] Critical to our

* To whom correspondence should be addressed.
[†] Department of Chemistry, The Pennsylvania State University.
[‡] Advanced Materials Lab, Sandia National Laboratories, Albuquerque, NM 87106.
[§] Departments of Chemistry and Materials Science and Engineering, The Pennsylvania State University.

10.1021/jp9921699 CCC: $18.00
Published on Web 09/04/1999

ability to make *quantitative* comparisons is having the molecules under study in identical conformations and chemical environments as discussed below. This was not the case in our earlier work utilizing two-dimensional matrix isolation of molecules under study.[27,28]

We use a two-component self-assembled monolayer (SAM) of alkanethiolates adsorbed on Au{111} as our model system. In ref 47 we demonstrated that we can create a mosaic structure with molecularly sharp boundaries between patches of the different component molecules.[47] Such well-defined physical structures are ideal for measuring electron transfer. Despite the volume of STM work on SAMs, the mechanism by which the molecular components are imaged remains poorly understood. We show that the STM contrast mechanism can be understood using a two layer tunnel junction model. Use of a two-dimensional mosaic structure with molecularly sharp boundaries allows an experimental test of this model. To eliminate any specific chemical effects which might cause STM contrast, we chose two alkanethiols with slightly different alkyl chain length, 1-decanethiol, $CH_3(CH_2)_9SH$, and 1-dodecanethiol, $CH_3(CH_2)_{11}SH$. The difference in film thickness between the 10-carbon 1-decanethiolate (**10**) and the 12-carbon 1-dodecanethiolate (**12**) SAM is 2.2 Å for an alkyl chain tilt angle of 30°.[47] Within ordered domains, these molecules adopt identical conformations and film structures,[48] including identical presentations of the terminal methyl groups which differ for odd and even alkyl chain lengths. Previous studies have demonstrated that surfaces can be produced with the mixed components[47,49−51] and that STM can molecularly resolve and differentiate the component molecules.

Experimental Section

We prepared a two-component mosaic SAM using a stepwise procedure as described in ref 47. Briefly, a single-component SAM of 100% **12** was prepared from a 1 mM solution of thiol of **12** in ethanol. The Au{111} was prepared by vapor depositing Au onto freshly cleaved heated muscovite mica. The substrate was immersed in the alkanethiol solution for 18 h, removed, rinsed thoroughly in solvents, and then blown dry with N_2. Then, this single component SAM of **12** was heated for 1 h in neat ethanol at 78 °C, cooled, rinsed, and blown dry. Finally, the SAM was immersed into a 1 mM solution of the thiol of **10** in ethanol at room temperature for 6 h, rinsed, and blown dry. The SAMs were imaged by STM using constant current feedback.[52] Our images were acquired with a tunnel junction transimpedance of 100 GΩ or greater, where the tip is outside the SAM so that the monolayer surface is not perturbed.[47,53] The scanning tunneling microscope was enclosed in a controlled atmosphere using a constant dry N_2 purge. Similar results have been obtained using other length alkanethiol combinations and component ratios.[51,54] All the STM images shown here are presented unfiltered.

Results and Discussion

Alkanethiols on Au{111} are known to form domains of ($\sqrt{3} \times \sqrt{3}$) R30° and related superstructures.[50] Figure 1A shows a STM topograph of the two-component mosaic SAM. The higher topographic (bright) regions are domains of **12**, present largely as well-ordered islands. The islands of **12** are surrounded by **10**, displaying defect densities typical of SAMs formed at room temperature. The roughly circular topographic depressions (darkest areas) within the domains of **10** are Au substrate vacancy islands, one-Au atomic layer deep pits in the Au substrate which are characteristic of room-temperature self-assembly.[50] Occasional molecules of **12** are observed in the regions of **10** and occasional molecules of **10** in the domains of **12**. Because the domains of **12** were treated at high temperature, the Au vacancy islands are not present within them.[47]

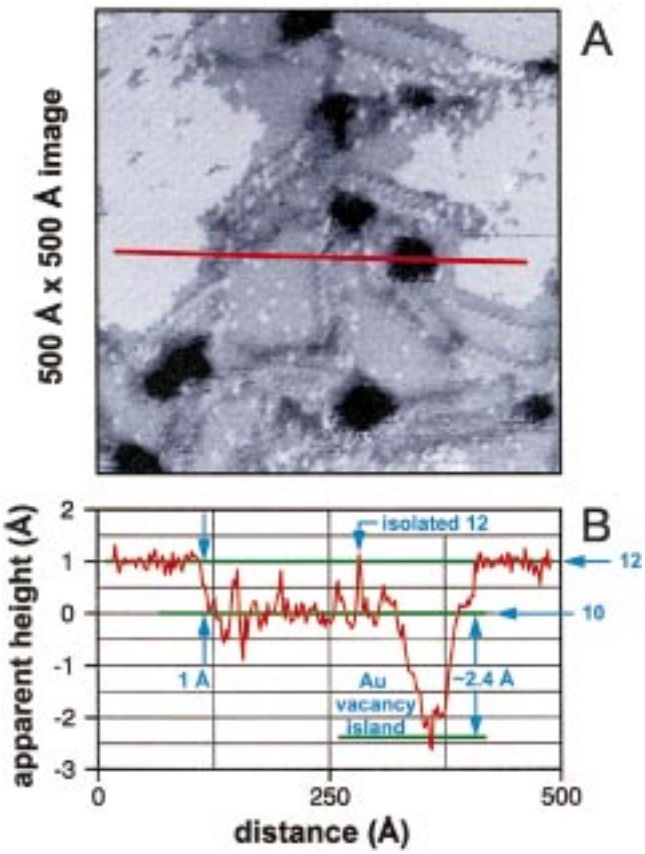

Figure 1. (A) STM image of a 500 Å × 500 Å area of the mixed composition mosaic SAM of **10** and **12** showing the alkanethiolate molecular lattice. The topographically higher (shown as brighter) regions are domains of **12**. These are present largely as well-ordered islands, remnants of the treatment in hot ethanol, which dramatically reduces the defect density. The islands of **12** are surrounded by the topographically lower **10**, displaying domain sizes and defect densities typical of SAMs formed at room temperature. These defects, the topographically lower (shown as darker) spots, are Au substrate vacancy islands (one atom deep depressions in the underlying Au{111} substrate) and the alkanethiolate structural domain boundaries (also darker). Interspersed molecules of **12** are observed in the regions of **10** and vice versa. The boundaries between the regions of **10** and **12** are well defined and are molecularly sharp. The image was recorded with a tip bias of +1.0 V and a tunneling current of 10 pA. (**B**) A topographic cross section extracted from **A** on the path shown by the red line. The STM topographic heights are shown for **12**, **10**, and a Au substrate vacancy island. Note that the height difference between the molecular terraces of **12** and **10** is 1.0 ± 0.2 Å, in contrast to the physical height difference of 2.2 Å. The cross section passes through a Au substrate vacancy island, 2.4 Å deep, and also through an isolated molecule of **12** in the **10** region.

A cross section extracted from this image (along the path indicated by the red line in Figure 1A) is shown in Figure 1B. The path was chosen so as to run between two molecular terraces of **12**, passing over an isolated molecule of **12** in the domain of **10** as well as a Au substrate vacancy island. The STM topographic height difference between the regions of **10** and **12** is 1.0 ± 0.2 Å. The isolated molecule of **12** appears at the same height as the full domains of **12**, but we observe that the apparent heights of these isolated molecules vary to some extent. This is also the case for monolayer films deposited from mixed solutions and is discussed further below.

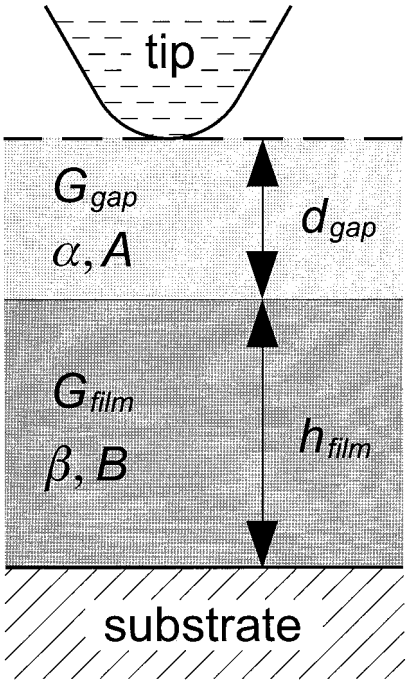

Figure 2. Two-layer tunnel junction model. The STM tunnel junction is composed of two distinct layers: the vacuum gap and the film. Each region is characterized by a transconductance, *G*, which is dependent on the physical thickness of the layer. The film thickness is an intrinsic property, while the vacuum gap thickness is controlled by the STM to maintain a constant overall transconductance.

We can use the STM height difference, Δh_{STM}, of these molecular terraces to determine the *difference* in tip−film−substrate electron transfer through each region. This is possible because the two molecules/regions can be imaged under identical conditions using the same STM tip. The height of a molecule measured by STM, h_{STM}, is not typically the same as the physical film thickness, h_{film} (e.g., from structural models), because the tip−sample interaction convolves electronic and physical structure.[45,46,52] Thus, the interpretation of images requires a knowledge of the specific sample. At the high tunnel junction transimpedances used for imaging the alkanethiolate molecular lattice, the tip is outside the film.[47] This results in a tunnel junction composed of two distinct layers (Figure 2): the film, with a thickness and a transconductance determined by its intrinsic properties, and the tip−film gap, with adjustable transconductance determined by its separation, d_{gap}, which is controlled by the scanning tunneling microscope, and the apparent tunneling barrier height, an intrinsic property of the film.[52,55] The constant-current STM topograph is a surface of constant tunneling current with height contributions from both the film and the tip−film gap; $h_{STM} = h_{film} + d_{gap}$. Note that we do not directly measure h_{STM} but rather Δh_{STM} between the molecular terraces of **10** and **12**.

For an understanding of how the alkyl chains contribute to the electron tunneling properties of SAMs, we can turn to the large body of experimental and theoretical work which has addressed the distance dependence of electron transfer kinetics through σ-bonded hydrocarbon bridges.[1−3,6−13,15,16,33,44,56,57] A general feature of these results under nonresonant tunneling conditions is that the transconductance decreases exponentially with increasing length. Experimental measurements include intramolecular donor−acceptor systems,[7−9] biochemical systems,[3,6] electrochemistry through alkanethiolate SAMs,[10−12,15] metal−insulator−metal junctions[16] and those by atomic force microscopy combined with a conducting probe tip.[33] These measurements show that electrons tunnel through these bridges with a rate, i_t, the tunneling current, which is proportional to $\exp(-\beta l)$, where l is the length of the bridge and β, the decay constant, ranges from 0.8 to 1.4 $Å^{-1}$ (1.0 to 1.8 per methylene bridge).[2,44] Theoretical calculations also predict that the interactions of the molecule with the electrodes (viz. the tip and the substrate) have very strong effects on the overall transconductance of the substrate−molecule−tip system.[56,57] Hence, the chemical nature of the interaction of the adsorbate with the surface is predicted to have a profound effect; chemisorption yields high transconductance, while physisorption yields low transconductance.[56,57] In our continuing work on this subject, we are exploring the effect of the variation in chemical contact on the transconductance.

Using this background, we can gain insight into the interpretation of STM topographs by examining the two-layer tunnel junction model presented in Figure 2. The transconductances, *G*, across each layer are

$$\text{vacuum gap:} \quad G_{gap} = A \exp(-\alpha d_{gap})$$

and

$$\text{film:} \quad G_{film} = B \exp(-\beta h_{film})$$

where α and β are the respective decay constants, d_{gap} and h_{film} are the layer thicknesses, and the prefactors, *A* and *B*, are the respective contact conductances.[57] Because the transconductance is an electron tunneling probability, as opposed to a dissipative current flow, the transconductance of the composite two-layer tunnel junction is the *product* of the transconductances of the individual layers, $G_t = G_{film}G_{gap}$. A thin film composed of two components (1 and 2) will have a different set of constants associated with each component. The scanning tunneling microscope operating with constant current feedback constrains G_t to be constant over the image, i.e., $G_t = G_{film1}G_{gap1} = G_{film2}G_{gap2} = i_t/e_t =$ constant, where e_t is the tunnel junction bias voltage. From our model, $\Delta h_{STM} \equiv h_{STM2} - h_{STM1} = (h_{film2} + d_{gap2}) - (h_{film1} + d_{gap1}) = \Delta h_{film} + \Delta d_{gap}$. Applying the simplifying and reasonable assumption that the characteristics of the vacuum gap do not change significantly from component 1 to 2 ($\alpha_1 \approx \alpha_2$, $A_1 \approx A_2$), and that the variation in β is also small ($\beta_1 \approx \beta_2$), we obtain

$$\Delta h_{STM} = \Delta h_{film}(1 - \beta/\alpha) + (1/\alpha) \ln(B_2/B_1) \qquad (1)$$

The first term shows that Δh_{STM} will have a linear dependence on Δh_{film}. The last term is an offset in STM topography due to the differences in the contact conductances of the two thin-film components which can be responsible for a nonzero Δh_{STM} even when $\Delta h_{film} = 0$. Clearly variations in the other constants, e.g., α and β, can also contribute to the Δh_{STM}. Because the molecular components **10** and **12** are members of a homologous series, the 1-alkanethiolates, are in identical conformations, present the same terminal functional group in the same conformation, and are measured with the same probe tip, we can reasonably assume that α, β, *A*, and *B* vary very little, if at all, between the different regions of the multicomponent film. Therefore, for our experimental system, we neglect the last term.

We note that in order to make such a direct comparison it is important to be able to hold constant the conformation and chemical environment of the molecules under study. An example of the effect of different conformation and environment can be seen at the structural domain boundaries shown in the STM

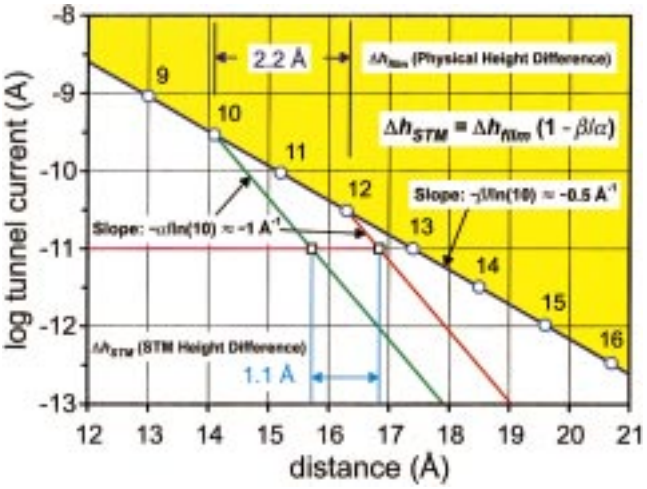

Figure 3. Semilogarithmic plot of the tunneling current vs tip−Au substrate separation for 1-alkanethiolates on Au{111} at a 1 V tip bias (adapted from ref 33). The open circles represent the hypothetical current−distance point for the tip just in contact with the ends of the alkyl chains with the total number of carbons indicated. These circles fall on a line with a slope $-\beta/\ln(10) = -0.5$ Å^{-1} ($\beta = 1.2$ Å^{-1} or 1.5 per methylene unit). The yellow region above this line corresponds to the condition where the tip has penetrated the alkanethiolate film. The lines intersecting the open circles at alkyl chain lengths of 10 (green) and 12 (red) carbon atoms, respectively, represent the tunneling current−distance relationship when the tip is outside the alkanethiolate film (above the ends of the alkanethiolate chains) with a slope of $-\alpha/\ln(10) = -1.0$ Å^{-1}. The tunneling current set-point value of 10 pA (magenta line) used for the data shown in Figure 1 positions the probe tip outside the films of both **10** and **12**.[47] The topographic height difference measured by STM is the distance between these two operating points, open squares. The relationship between the STM height difference Δh_{STM} and the physical height difference Δh_{film} is $\Delta h_{STM} = \Delta h_{film}(1 - \beta/\alpha)$, which for this diagram is $\Delta h_{STM} \approx 0.5\Delta h_{film}$.

image of a single-component monolayer in ref 47 (see the feature marked by the arrow in Figure 1B of ref 47).

Theoretical estimates of the electronic transmission coefficients for tunneling directly through alkanethiolate molecules have been reported by Sautet and co-workers.[33] If the two-layer tunnel junction model were correct, their transmission coefficients should allow accurate prediction of our observed STM height differences. To test this, we have applied Sautet and coworkers' values to the tunneling conditions used to record the data shown in Figure 1A. The predicted results are (1) the transconductance of the alkanethiolate chain decreases by an order of magnitude for every two additional methylene units in the chain ($\beta \approx 1.2$ Å^{-1}) and (2) while the tip is outside the SAM, the transconductance of the tunnel junction decreases an order of magnitude for each additional angstrom of tip−film separation ($\alpha \approx 2.3$ Å^{-1}). These results are shown graphically in Figure 3 as a semilogarithmic plot of the tunneling current vs tip−sample separation. The open circles represent the hypothetical condition where the tip is just in contact with the end of the chain for the number of carbon atoms in the molecule as indicated. These points fall on a line with slope $-\beta/\ln(10)$. Points inside the yellow region correspond to the case where the tip has penetrated the SAM. Here, we only consider the case where the tip is outside the exposed SAM interface. We note that it is for tunneling transconductances at and above this value that we lose the ability to resolve the molecular lattice for a given alkyl chain length.[47] Outside the film, the current−distance dependence is expressed by the decay constant, α, which is related to the work function of the SAM, ϕ, and the electron mass, m, by $\alpha = (8m\phi)^{1/2}/\hbar$. We assume that the work function of the SAMs is approximately independent of the alkyl

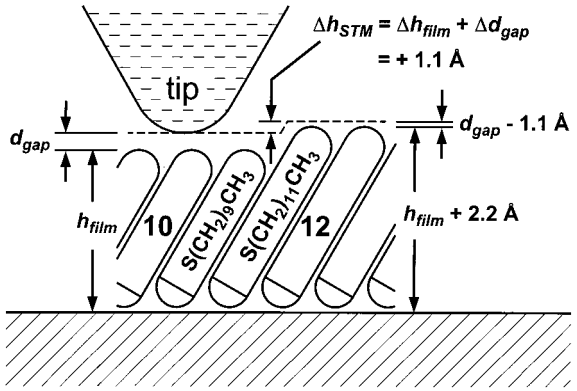

Figure 4. Schematic diagram of a molecularly sharp **10**/**12** boundary showing the STM tip trajectory (dashed line) corresponding to the constant tunneling current operating point 5 in Figure 1. The STM tunnel junction is composed of two regions, the film and the tip−film gap. The STM topographic height, h_{STM}, is the sum of the physical height, h_{film}, and the tip−film gap, d_{gap}. As the STM scans from the **10** region to the **12** region, h_{film} increases 2.2 Å and the film transconductance decreases 10-fold. To compensate, the STM decreases d_{gap} 1.1 Å to increase the tip−film gap transconductance 10-fold, thereby maintaining a constant overall tunnel junction transconductance. Consequently $\Delta h_{STM} = \Delta h_{film} + \Delta d_{gap} = +1.1$ Å.

chain length.[33] This gives a family of curves each beginning at the open circle corresponding to the number of carbon atoms in the respective alkanethiolate. These are shown for **10** (green) and **12** (red). The slopes of these curves can be measured independently by dithering the tip−sample separation and measuring the change in current. This yields a measure of the apparent tunneling barrier height and thus α.[47,52,55]

The scanning tunneling microscope operating point is the tip−sample distance for a given tunneling current and is unique for each alkanethiolate. Operating points outside the film within domains of **10** and **12** (open squares) can be found from the intersection of the 10 pA tunneling current value (magenta line) used to record the data shown in Figure 1A and the respective current−distance curves. The distance between these two operating points is Δh_{STM}. Using our approximation for eq 1, the relationship between Δh_{STM} and Δh_{film} is

$$\Delta h_{STM} = \Delta h_{film}(1 - \beta/\alpha) \qquad (2)$$

In this instance, the prediction is that $\Delta h_{STM} \approx 0.5\Delta h_{film}$. The plot shows for our STM conditions the apparent height difference would be 1.1 Å. In excellent agreement, we observe apparent height differences between domains of **10** and **12** of $\Delta h_{STM} = 1.0 \pm 0.2$ Å. This is depicted schematically in Figure 4 for the STM tip trajectory over a molecularly sharp **10**/**12** boundary at constant tunneling current. As the scanning tunneling microscope scans from the region of **10** to the region of **12**, h_{film} increases 2.2 Å while the film transconductance decreases 10-fold. To compensate, the scanning tunneling microscope decreases d_{gap} by 1.1 Å to increase the tip−film gap transconductance 10-fold, thereby maintaining a constant overall tunnel junction transconductance. Consequently, $\Delta h_{STM} = \Delta h_{film} + \Delta d_{gap} = +1.1$ Å.

We measure Δh_{STM} between molecular terraces of the two molecules under study because this gives us the limiting values of the measured height differences. The actual values of Δh_{STM} obtained for isolated molecules vary to some extent, but are limited by the values found for separated domains. We attribute these variations as being due to the STM tip resolution.

The diagram presented in Figure 3 provides a simple graphical relationship between the STM topographic heights and the

electronic and physical structure of the surface. Therefore, it is instructive to examine a few special cases. When the conductivity of the film is independent of its thickness ($\beta = 0$), then $\Delta h_{STM} \approx \Delta h_{film}$. This case corresponds to highly conducting films, e.g., the Au substrate itself, where the STM topographic height difference is identical to the physical height difference. If $\alpha = \beta$, the current−distance dependence of electron tunneling through the film is identical to the current−distance dependence of electron tunneling through the tip−film gap; thus, $\Delta h_{STM} = 0$ and *no* topography due to the film will be observed by STM. For $0 < \beta/\alpha < 1$, the case depicted in Figure 3, the STM topographic height difference will be less than the physical height difference, $0 < \Delta h_{STM} < \Delta h_{film}$. The final case is a curious one; for $\beta/\alpha > 1$, the tunneling current decays more rapidly with distance inside the film than it does in the tip−film gap causing the STM topography to appear inverted, $\Delta h_{STM} \propto -\Delta h_{film}$. This instance can arise when the film is immersed in a medium, such as a liquid which has a smaller decay constant than the film, or if the apparent tunneling barrier height over the film is very low. Cases where α and/or β are negative correspond to unphysical situations.

We can use this treatment to obtain quantitative comparisons between classes of chemical compounds and chemical contacts in terms of their transconductances. Both contributions to the transconductance are equally important because the transconductance is the *product* of the contact conductance and the (through-film) exponential decay factor. Chemical backbones with lower slopes (β values) in plots such as that shown in Figure 3 have been measured.[4,6,14] However, a lower β does not necessarily signify a higher transconductance. Although a low β is a desirable property for molecular wires, it is a necessary but not sufficient condition for high transconductance molecular wires. By comparing the intercepts for lines extrapolated to zero chain lengths of different backbone-chemical contact combinations, we can evaluate the contribution of different chemical contacts to the transconductance. We are currently exploring the effects of both backbone and chemical contact on transconductance.

In these experiments, we have not measured the extent to which there is electronic coupling between adjacent molecules. It would be interesting to know the extent to which the measured transconductance is due to the backbones of the (tilted) chains or simply to the thickness of the film.[60] One approach may be to determine the effective coupling by measuring the perturbations of the apparent transconductances of molecules adjacent to a molecule inserted with identical structure but (known) higher or lower transconductance either due to backbone or contact variations.

Conclusions

We are able to compare the transconductance of these molecules accurately using STM because the molecularly sharp **10**/**12** boundaries of the mosaic SAM enables the imaging of ordered domains in the identical conformation within the same image using the same STM probe tip. It is a necessary condition for imaging these films that the STM probe tip remains outside the film, which is achieved by using a low tunnel junction transconductance ($\lesssim 10^{-11}\ \Omega^{-1}$), as can be seen in Figure 3. The STM tunneling junction is then composed of two layers, the film and the tip−film gap. The film is imaged with constant tunneling current where the scanning tunneling microscope constrains the tunnel junction transconductance to be constant by changing the tip−film gap to compensate for changes in film transconductance and film thickness. The transconductance of the molecules of the film are exponentially dependent on their length with the decay constant β and a preexponential factor B, while that of the tip−film gap depends on α and A. Because **10** and **12** are from a homologous series, the 1-alkanethiols, we can assume that β, B, α, and A are the same for both **10** and **12**. The transconductance of **10** is 10-fold higher than that of **12** because it is shorter (two methylene units). The STM measured **10**/**12** height difference is less than the actual physical height difference because it convolves the physical and the electronic properties of the film into a surface of constant tunneling current—the STM constant-current topograph.

We have shown that the measured values of electron transfer can be connected quantitatively with widespread transconduction phenomena of molecular frameworks and films. STM has the advantage that both the driving force and the tunneling distance can be varied independently for studies of electron transfer through single molecules and molecular assemblies. We are working toward quantifying the conductivity of inserted conjugated molecules[27] and of related films and the effects of chemical substitutions on electron transfer properties.

Acknowledgment. We thank P. Sautet, C. Joachim, A. Nitzan, M. Salmeron, and D. Yaron for valuable discussions. The support of the National Science Foundation, the Office of Naval Research, the Defense Advanced Research Projects Agency, the Alfred P. Sloan Foundation, and the John Simon Guggenheim Memorial Foundation are gratefully acknowledged.

References and Notes

(1) Barbara, P. F.; Meyer, T. J.; Ratner, M. A. *J. Phys. Chem.* **1996**, *100*, 13148−13168.

(2) Arnaut, L. G.; Formosinho, S. J. *J. Photochem. Photobiol. A: Chem.* **1996**, *100*, 15−34.

(3) Moser, C. C.; Keske, J. M.; Warncke, K.; Farid, R. S.; Dutton, J. P. *Nature* **1992**, *355*, 796−802.

(4) Holmlin, R. E.; Dandliker, P. J.; Barton, J. K. *Angew. Chem., Int. Ed. Engl.* **1997**, *36*, 2714−2730.

(5) Grätzel, M. *Heterogeneous Photochemical Electron Transfer*; CRC Press: Boca Raton, 1989.

(6) Gray, H. B.; Winkler, J. R. *Annu. Rev. Biochem.* **1996**, *65*, 537−561.

(7) Closs, G. L.; Miller, J. R. *Science* **1988**, *240*, 440−447.

(8) Paddon-Row, M. N.; Oliver, A. M.; Warman, J. M.; Smit, K. J.; de Haas, M. P.; Oevering, H.; Verhoeven, J. W. *J. Phys. Chem.* **1988**, *92*, 6958−6962.

(9) Paulson, B.; Pramod, K.; Eaton, P.; Closs, G.; Miller, J. R. *J. Phys. Chem.* **1993**, *97*, 13042−13045.

(10) Chidsey, C. E. D. *Science* **1991**, *251*, 919−922.

(11) Miller, C.; Cuendet, P.; Grätzel, M. *J. Phys. Chem.* **1991**, *95*, 877−886.

(12) Finklea, H. O.; Liu, L.; Ravenscroft, M. S.; Punturi, S. *J. Phys. Chem.* **1996**, *100*, 18852−18858.

(13) Li, T. T.-T.; Weaver, M. J. *J. Am. Chem. Soc.* **1984**, *106*, 6107−6108.

(14) Sachs, S. B.; Dudek, S. P.; Hsung, R. P.; Sita, L. R.; Smalley, J. F.; Newton, M. D.; Feldberg, S. W.; Chidsey, C. E. D. *J. Am. Chem. Soc.* **1997**, *119*, 10563−10564.

(15) Carter, M. T.; Rowe, G. K.; Richardson, J. N.; Tender, L. M.; Terrill, R. H.; Murray, R. W. *J. Am. Chem. Soc.* **1995**, *117*, 2896−2899.

(16) Polymeropoulos, E. E.; Sagiv, J. *J. Chem. Phys.* **1978**, *69*, 1863−1847.

(17) Reed, M. A.; Zhou, C.; Muller, C. J.; Burgin, T. P.; Tour, J. M. *Science* **1997**, *278*, 252−253.

(18) Zhou, C.; Deshpande, M. R.; Reed, M. A.; Jones, L., II; Tour, J. M. *Appl. Phys. Lett.* **1997**, *71*, 611−613.

(19) Andres, R. P.; Bein, T.; Dorogi, M.; Feng, S.; Henderson, J. I.; Kubiak, C. P.; Mahoney, W.; Osifchin, R. G.; Reifenberger, R. *Science* **1996**, *272*, 1323−1325.

(20) Andres, R. P.; Bielefeld, J. D.; Henderson, J. I.; Janes, D. B.; Kolagunta, V. R.; Kubiak, C. P.; Mahoney, W. J.; Osifchin, R. G. *Science* **1996**, *273*, 1690−1691.

(21) Tans, S. J.; Thess, A.; Geerligs, L. J.; Smalley, R. E. *Nature* **1997**, *386*, 474−476.

(22) Langer, L.; Bayot, V.; Grivei, E.; Issi, J.-P.; Heremans, J. P.; Olk, C. H.; Stockman, L.; Van Haesendonck, C.; Bruynseraede, Y. *Phys. Rev. Lett.* **1996**, *76*, 479−482.
(23) Ebbesen, T. W.; Lezec, H. J.; Hiura, H.; Bennett, J. W.; Ghaemi, H. F.; Thio, T. *Nature* **1996**, *382*, 54−56.
(24) Dai, H.; Wong, E. W.; Lieber, C. M. *Science* **1996**, *272*, 523−526.
(25) Martel, R.; Shea, H. R.; Avouris, P. *Nature* **1999**, *398*, 299.
(26) Thess, A.; Lee, R.; Nikolaev, P.; Dai, H.; Petit, P.; Robert, J.; Xu, C.; Lee, Y. H.; Kim, S. G.; Rinzler, A. G.; Colbert, D. T.; Scuseria, G. E.; Tománek, D.; Fischer, J. E.; Smalley, R. E. *Science* **1996**, *273*, 483−487.
(27) Bumm, L. A.; Arnold, J. J.; Cygan, M. T.; Dunbar, T. D.; Burgin, T. P.; Jones, L., II; Allara, D. L.; Weiss, P. S. *Science* **1996**, *271*, 1705−1707.
(28) Cygan, M. T.; Dunbar, T. D.; Arnold, J. J.; Bumm, L. A.; Shedlock, N. F.; Burgin, T. P.; Jones, L., II; Allara, D. L.; Tour, J. M.; Weiss, P. S. *J. Am. Chem. Soc.* **1998**, *120*, 2721−2732.
(29) Joachim, C.; Gimzewski, J. K.; Schlittler, R. R.; Chavy, C. *Phys. Rev. Lett.* **1995**, *74*, 2102−2105.
(30) Joachim, C.; Gimzewski, J. K. *Chem. Phys. Lett.* **1997**, *265*, 353−357.
(31) Yazdani, A.; Eigler, D. M.; Lang, N. D. *Science* **1996**, *272*, 1921−1924.
(32) Eigler, D. M.; Weiss, P. S.; Schweizer, E. K.; Lang, N. D. *Phys. Rev. Lett.* **1991**, *66*, 1189−1192.
(33) Salmeron, M.; Neubauer, G.; Folch, A.; Tomitori, M.; Ogletree, D. F.; Sautet, P. *Langmuir* **1993**, *9*, 3600−3611.
(34) Datta, S.; Tian, W.; Hong, S.; Reifenberger, R.; Henderson, J. I.; Kubiak, C. P. *Phys. Rev. Lett.* **1997**, *79*, 2530−2533.
(35) Samanta, M. P.; Tian, W.; Datta, S.; Henderson, J. I.; Kubiak, C. P. *Phys. Rev. B* **1996**, *53*, R7626−R7629.
(36) *Photoinduced Electron Transfer*; Fox, M. A., Chanon, M., Eds.; Elsevier Science Publishers: Amsterdam, 1988.
(37) *An Introduction to Molecular Electronics*; Petty, M. C., Bryce, M. R., Bloor, D., Eds.; Oxford University Press: New York, 1995.
(38) *Molecular Electronics: Science and Technology*; Aviram, A., Ed.; Conference Proceedings No. 262; American Institute of Physics: New York, 1992.
(39) *Nanostructure Physics and Fabrication*; Reed, M. A., Kirk, W. P., Eds.; Academic Press: New York, 1989.
(40) *Nanostructures and Mesoscopic Systems*; Reed, M. A., Kirk, W. P., Eds.; Academic Press: New York, 1992.
(41) *Molecular Electronic Devices II*; Carter, F. L., Ed.; Marcel Dekker: New York, 1987.
(42) Miller, J. S. *Adv. Mater.* **1990**, *2*, 378−379, 495−497, 601−603.
(43) Joachim, C. *New J. Chem.* **1991**, *15*, 223−229.
(44) Hsu, C.-P.; Marcus, R. A. *J. Chem. Phys.* **1997**, *106*, 584−598.
(45) Sautet, P. *Chem. Rev.* **1997**, *97*, 1097−1116 and references therein.
(46) Van Hove, M. A.; Cerda, J.; Sautet, P.; Bocquet, M.-L.; Salmeron, M. *Prog. Surf. Sci.* **1997**, *54*, 315−329.
(47) Bumm, L. A.; Arnold, J. J.; Charles, L. F.; Dunbar, T. D.; Allara, D. L.; Weiss, P. S. *J. Am. Chem. Soc.*, in press.
(48) Dubois, L. H.; Nuzzo, R. G. *Annu. Rev. Phys. Chem.* **1992**, *43*, 437−463.
(49) Stranick, S. J.; Parikh, A. N.; Tao, Y.-T.; Allara, D. L.; Weiss, P. S. *J. Phys. Chem.* **1994**, *98*, 7636−7646.
(50) Poirier, G. E. *Chem. Rev.* **1997**, *97*, 1117−1127 and references therein.
(51) Arnold, J. J. M.S. Thesis, The Pennsylvania State University, University Park, PA, 1997.
(52) See, for example: Chen, C. J. *Introduction to Scanning Tunneling Microscopy*; Oxford University Press: New York, 1993. Weisendanger, R. *Scanning Probe Microscopy and Spectroscopy*; Cambridge University Press: New York, 1994.
(53) Schönenberger, C.; Jorritsma, J.; Sondag-Huethorst, J. A. M.; Fokkink, L. G. J. *J. Phys. Chem.* **1995**, *99*, 3259−3271.
(54) Charles, L. F.; Bumm, L. A.; Arnold, J. J.; Dunbar, T. D.; Allara, D. L.; Weiss, P. S. Manuscript in preparation.
(55) Olesen, L.; Brandbyge, M.; Sørensen, M. R.; Jacobsen, K. W.; Lægsgaard, E.; Stensgaard, I.; Besenbacher. F. *Phys. Rev. Lett.* **1996**, *76*, 1485−1488.
(56) Joachim, C.; Vinuesa, J. F. *Europhys. Lett.* **1996**, *33*, 635−640.
(57) Magoga, M.; Joachim, C. *Phys. Rev. B* **1997**, *56*, 4722−4729.
(58) Laibinis, P. E.; Whitesides, G. M.; Allara, D. L.; Tao, Y.-T.; Parikh, A. N.; Nuzzo, R. G. *J. Am. Chem. Soc.* **1991**, *113*, 7152−7167.
(59) Cygan, M. T. Ph.D. Thesis, The Pennsylvania State University, University Park, PA, 1997.
(60) One qualitative clue on this front is that matrix-isolated bundled molecules of phenylene−ethynylene oligomers appeared to have higher microwave conductivity than isolated single molecules in the experiments presented in refs 27 and 28. This assignment is not unambiguous, however, as the effects of chemical environment and intermolecular electronic coupling are not separable.